https://dx.doi.org/10.4314/ijs.v26i3.15

HYDROGEOPHYSICAL EXPLORATION AND GROUNDWATER QUALITY ASSESSMENT OF OBADA OKO, OGUN STATE, NIGERIA

Makinde, V.[1], Ganiyu, S. A.[1], Bada, B. S.[2], Salawu, A. O.[1,*], Ifeyemi, O. A.[1] and Odutayo, J. O.[3]

[1]Department of Physics, Federal University of Agriculture, Abeokuta, Ogun State, Nigeria.

[2]Department of Environmental Management and Toxicology, Federal University of Agriculture, Abeokuta, Ogun State, Nigeria.

[3]Department of Biomedical Physics, University of Aberdeen, Scotland, United Kingdom.

[*]Corresponding Author's Email: biodunsalawu@yahoo.com

(Received: 23rd February, 2024; Accepted: 15th November, 2024)

ABSTRACT

Water is one of the prime necessities of life for the survival of man and a host of other living things. Access to potable water supply over the years has been difficult in developing countries leading to high rates of water borne diseases, hence the need to assess the hydrogeological potential of Obada-Oko in Ewekoro Local Government Area of Ogun State. The study investigated aquifer distribution and locations of possible sites where boreholes and hand-dug wells could be drilled for potable and uncontaminated groundwater supply. The study area falls within a transition zone between sedimentary and basement complex rocks of southwestern Nigeria. Vertical Electrical Sounding (VES) and 2-Dimensional Electrical Resistivity Tomography (2D ERT) surveys were carried out using Schlumberger and Wenner arrays respectively. Resistivity data were acquired using Campus Tigre resistivity meter at twelve VES points and six 2D traverses of lengths varying from 100 to 150 m. The resistivity data obtained from 2D ERT were inverted using RES2DINV software while IPI2WIN and WinResist software were used for VES data interpretation. A maximum of five geoelectric layers namely: topsoil, clayey soil, clayey sand, sandy soil, weathered/fractured and fresh basement were delineated beneath the traverses. The weathered and fractured layers had resistivity varying from 20 to 690 Ωm and thickness varying from 12 to 27 m. The 2D ERT models showed three layers: top layer, weathered layer and fresh basement. The topsoil thickness varies from 1 to 10 m while fractured/fresh basement layer thickness vary between 6 and 13 m. The maximum depth of penetration of 2D ERT and VES were 13 m and 31 m respectively. Productive hand-dug wells/boreholes could be sited on traverses 2, 3 and 6; VES points 6 and 12 were suspected to have high groundwater potential. Though the longitudinal conductance values revealed protective capacity rating to be mostly within poor category, which made the aquifer system highly vulnerable to contamination. Physical and chemical results of analyzed water samples fell within permissible limit of World Health Organization (WHO) and Nigerian Standard for Drinking Water Quality (NSDWQ) limit for drinking purposes. Piper trilinear diagram interpretation showed calcium and chloride to be the dominant cation and anion respectively. Groundwater potential tends to be high in five locations in the study area with suitable aquiferous media for groundwater extraction.

Keywords: Hydrogeological potential, Aquifer, Groundwater, Transition zone, Resistivity, Longitudinal conductance.

INTRODUCTION

Safe drinking water is essential to human health as it is devoid of pollution in any form. Global access to safe drinking water has significantly improved over the last few decades with advances in water treatment technologies, infrastructure development, and public health initiatives. This has contributed to safer water supplies in many regions, but about one billion people still lack access to safe water and over 2.5 billion people do not have access to adequate sanitation (UNICEF, 2012). It has been estimated by observers that by the year 2025, water-related vulnerability will affect around half of the world's population (Kulshreshtha, 1998 & Boretti and Rosa, 2019). According to UN, 2009, certain emerging parts of the world's water demand would be 50% more than its supply by the year 2030. Using surface water resources is the simplest and most practical way to fulfil home water demand. Less than 0.01% of the world's total water and less than 2% of the fresh water in rivers, lakes, and other bodies of water are available for human use (Hamill and Bell, 1986). The bulk of the fresh water on Earth comes from groundwater, which is widely dispersed (Sillanpää and Shestakova, 2017). It offers a

relatively consistent supply that is unlikely to run out under normal circumstances, unlike surface sources, and is frequently in rather large quantities (*Alley et al., 1999)*. Groundwater accounts for approximately 95% of the freshwater on our planet (Morris *et al.,* 2003). Groundwater can be found under the surface of the earth in soil pore spaces as well as cracks in rock formations; an aquifer is a unit of rock or an unconsolidated deposit that can supply a usable amount of water (Greenburg, 2005). The surface below which soil pore spaces or cracks and cavities in rock become completely saturated with water is referred to as the water table. Groundwater is replenished naturally through a process known as recharge, which occurs when rainwater, snowmelt, or surface water seeps through the soil and permeable rock layers, eventually reaching underground aquifers. Groundwater is frequently extracted purposely for agriculture to irrigate fields, municipal and commercial or industrial usage by construction and operation of wells. Hydrogeology is an investigation of groundwater distribution and flow (Schnug *et al*., 2019). Hydrogeophysical investigations give details which may be utilised to gain insights into complicated hydrological processes, as input data for flow and transport models, and as a guide in the management of subsurface water resources and pollutants (Sassen *et. al.,* 2012). Geophysical techniques have been used in the exploration of minerals for more than 300 years, commencing about 1640 in Sweden with the use of magnetic compasses to explore iron ore. In 1800's, the search for base metals led to resistivity measurements, and by 1900's, Self Potential (SP) and resistivity were used by Schlumberger brothers for mineral prospecting (Zonge, 1993). Geophysical prospecting techniques based on the analysis of physical fields include electrical, magnetic, thermal elastic vibration, magnetic, and radioactive radiation (Kearey *et al.,* 2002). The measurements of these fields parameters are acquired on surface of the earth (land and water), in the air, and underground (shafts and wells). Location of ore bodies, geological formations, to mention a few and their fundamental characteristics are determined by the information obtained. This permits the choice of the most appropriate techniques for costly mining and drilling activities, hence improving their effectiveness. Several methods have been adopted for groundwater exploration in Ewekoro, Ogun State, Southwest and other parts of Nigeria (Jimoh *et al*., 2015; Badmus and Olatinsu, 2012). Electrical resistivity methods have been used to investigate groundwater in various lithological environments because the equipment is simple, field arrangement is easy and data interpretation is straightforward in contrast to alternative approaches (Ariyo and Banjo 2008, Ufoegbune *et al.,* 2009, Alile *et al.,* 2012, Ishola *et al.,* 2016). Electrical resistivity techniques are geophysical surveying techniques that help in visualizing the subsurface. They utilize variations in electric potential to identify materials in the subsurface. Resistivity is basically connected to Ohm's Law measuring Resistance. Resistance is computed by dividing the voltage by the current ($R = \frac{V}{I}$), a material's resistance value relies upon the material's resistivity (Marshall, 2018). Resistivity is defined as the measure of a material's ability to resist the passage of a current. The three principal methods of electric resistivity surveys concept are electric profiling, electric imaging and Vertical Electric Sounding (VES). This research work was aimed to investigate the aquifer distribution within Obada-Oko and locate possible sites where boreholes and hand-dug wells could be drilled for potable and uncontaminated groundwater supply. There was need to also determine the apparent resistivity of the area of study, examine the susceptibility of the aquifer in the area to pollution and determine the groundwater quality for drinking purposes.

LOCATION AND GEOLOGY OF THE STUDY AREA

Obada-Oko community is situated along old Abeokuta-Lagos Expressway. It lies within latitudes 7^0 03' and 7^0 05' North and longitudes 3^0 17' and 3^0 19' East (Figure 1). The study area is situated within Ewekoro Local Government Area (LGA) of Ogun State with land area of 63.5 km^2 (Odunaya, 2012). The Local Government Area is bounded by Abeokuta in the north, Ifo in the south, Obafemi-Owode in the east and Yewa in the west.

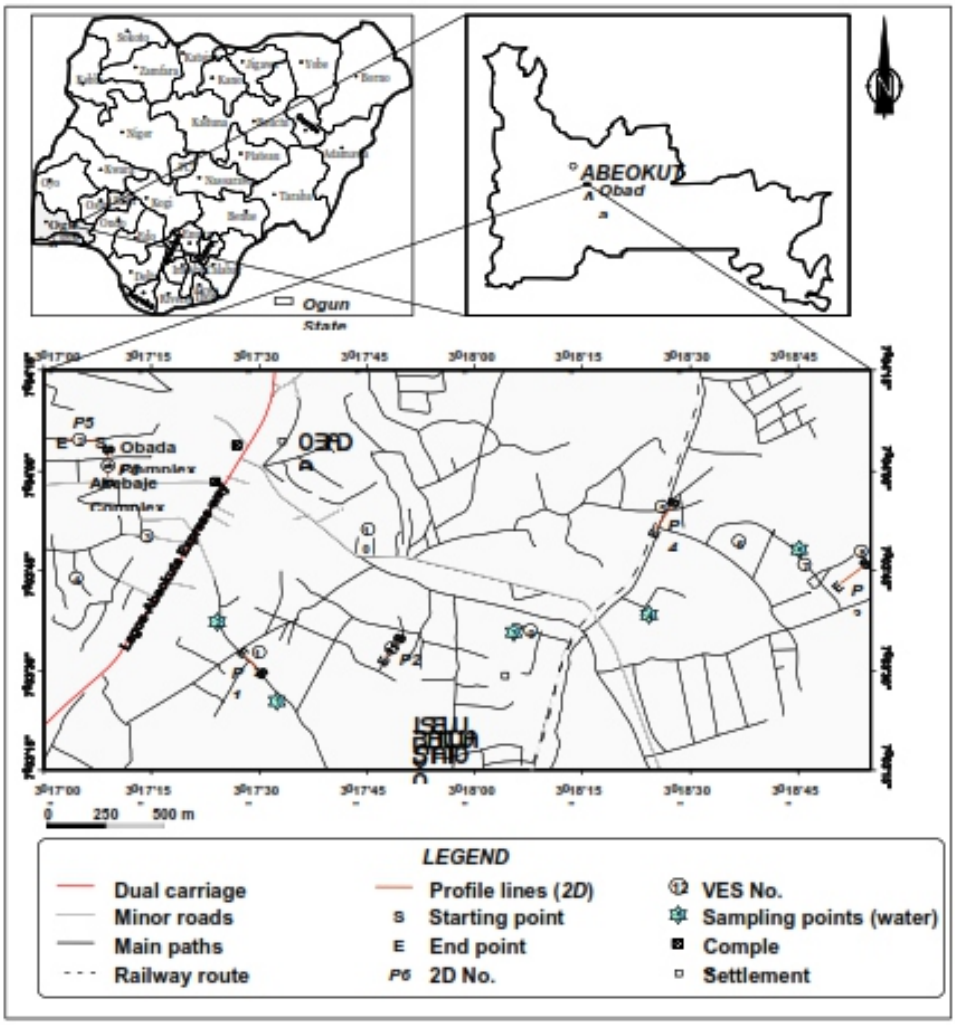

Figure 1. Location/Accessibility Map showing the Study Area's location.

Geologically, the study area is located in a transition zone; between sedimentary and basement complex rock of southwestern Nigeria (Figure 2). The sedimentary sequence of rocks in the study area is within the formation of Abeokuta, which comprise of sandstone and limestone (Ogunsanwo *et al.*, 2019). The Abeokuta formation is the Dahomey basin's oldest sedimentary unit (Oli *et al.,* 2019). It lies unconformably on the basement complex of southwestern which consists of coarsely grained, lower cretaceous and poorly sorted micaceous sandstone with inter-bedded mud-stone. It is surrounded by finer detrital sandstones, shales and siltstones that exhibit a transitional nature (Adabanija, 2012).

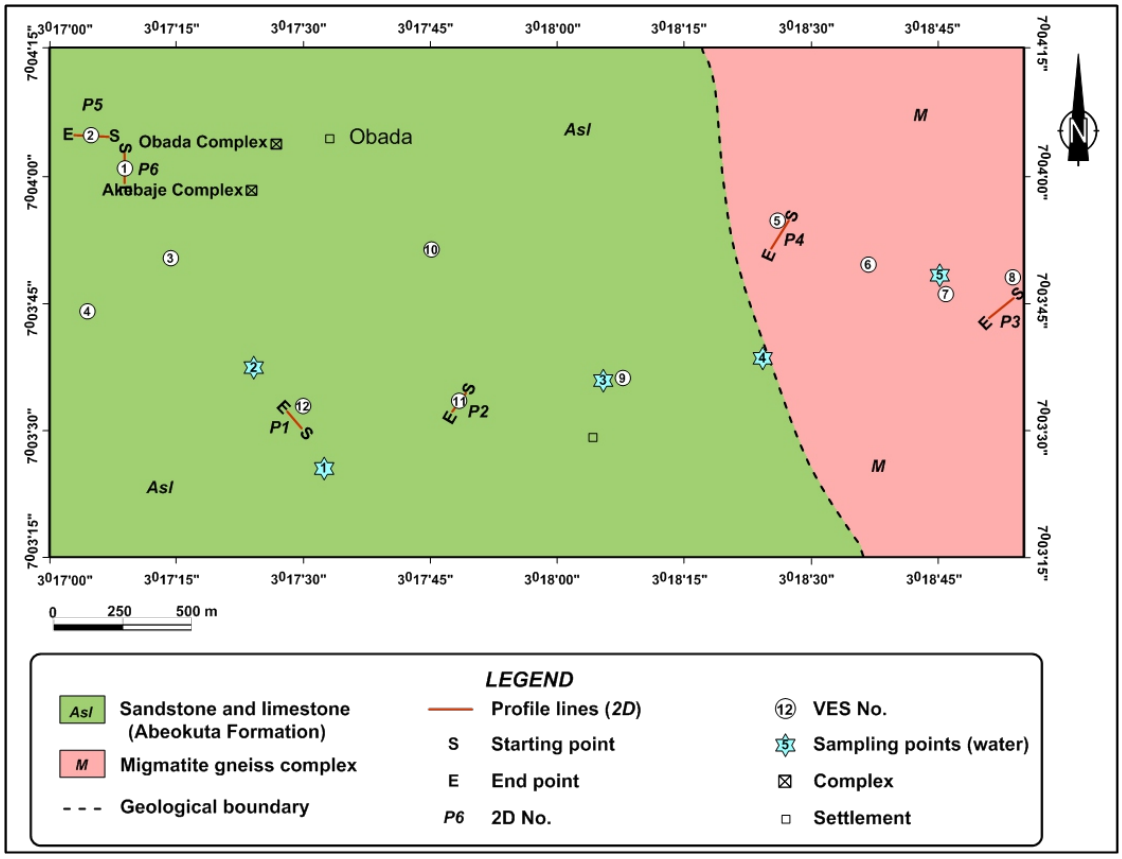

Figure 2. Geological Map displaying the Rock Types that underlies the Study Area.

The basement complex rock is made up of migmatite gneiss. Migmatites are diverse metamorphic rocks which consist of mixed mesosomes, melanosomes and leucosomes. They are partially melted continental crust's rock which consists of two components, the paleosomes and neosomes (Jimoh *et al.*, 2015). Odeyemi and Rahaman (1992) assumed that the meta-supracrustal rocks and migmatite-gneiss of the basement complex mark the end of Precambrian activity in Southwest Nigeria. Migmatite gneiss complex is the most widespread, oldest, and abundant rock type in the basement complex. Migmatite gneiss has grey colour and the texture medium grained, with interchange of mafic and felsic bands set in a medium to coarse grained ground mass.

METHODOLOGY

2-Dimensional Electrical Resistivity Tomography (2D ERT)

The basis of ERT technique comprises of the application of a steady direct current which is impressed into the ground via pair of electrodes and taking measurement of the resulting potential differences at another pair of electrodes (Figure 3). The process is established on multiple electrode and cable system (Metwaly and Alfouzan, 2013). 2-D ERT process is very fast and cost effective, which measures both straight and perpendicular changes in the subsurface resistivity (Ravindran and Prabhu, 2012).

In this study, resistivity data were obtained using Campus Tigre Terameter along six traverses. The traverses were oriented along E-S azimuth with traverse length varying from 100 and 150 m. Electrical resistivity data using Wenner electrode configuration of 5 m electrode spacing with a maximum spacing of 25 m were acquired on each of the six traverses.

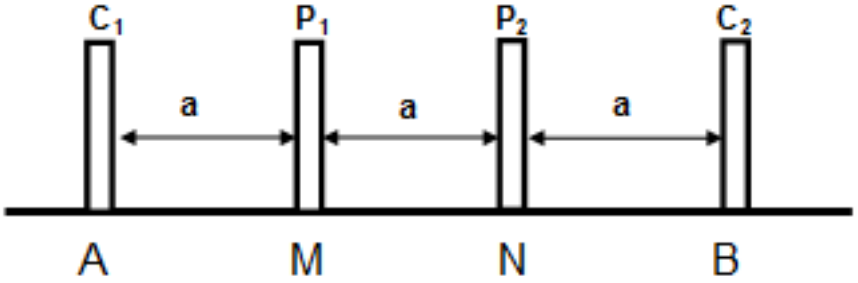

Figure 3. Wenner array configuration, sounding depth controlled by distance.

The geometric factor, G for the Wenner configuration is given as

$G = 2\pi a.$ (1)

In the Wenner array configuration, distances AM = MN = NB = a (2)

The apparent resistivity for Wenner array is therefore

$\varrho_a = 2\pi a \left(\frac{V}{I}\right)$ (3)

Wenner array generally provides great horizontally layer resolution, depth sensitivity together with high ratios of noise to signal. Contrarily, lateral location of deep inhomogeneities cannot be properly determined using Wenner array because potential electrodes and the large *a*-spacing degrade lateral clarity, and are situated within the current electrodes' range (Ward, 1990).

Data acquired using the Wenner array configuration from each survey line were separately inverted with the aid of RES2DINV computer Software as suggested by Loke and Barker (1996) to produce the 2-D resistivity models.

Vertical Electric Sounding (VES)

Twelve Schlumberger VES were acquired in the study area. The current electrode ($^{AB}/_{2}$) spacing vary from 1.0 m to 100.0 m while the potential electrode spacing ($^{MN}/_{2}$) varied from 0.25 m and 5.00 m. Schlumberger array (Figure 4) is related to the Wenner array. The major difference in terms of distribution geometry is the separation distance between potential electrodes (MN). It is not equal to half the separation distance between the electrode (AB) when compared with Wenner array.

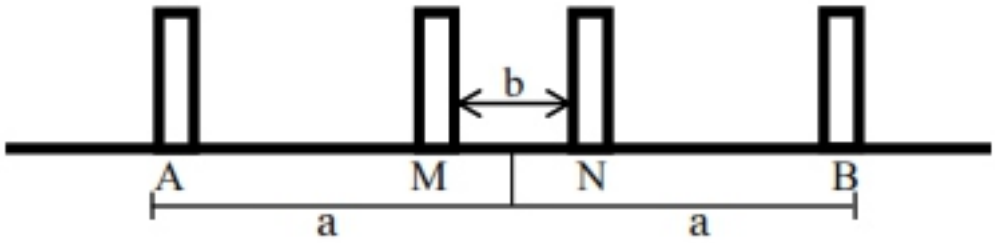

Figure 4. Schlumberger array with potential electrodes M and N, and, current electrodes A and B.

The calculations of apparent resistivity are somewhat heterogeneous and the data plotted are representation of apparent resistivity as a function of AB/2.

From Figure 4,

$AM = \frac{a-b}{2}$ (4)

$BM = \frac{a+b}{2}$ (5)

$AN = \frac{a+b}{2}$ (6)

$BN = \frac{a+b}{2}$ (7)

Therefore,

$$G = \frac{2\pi}{\left\{\left(\frac{1}{AM}\right) - \left(\frac{1}{BM}\right) - \left(\frac{1}{AN}\right) + \left(\frac{1}{BN}\right)\right\}} \quad (8)$$

Hence, $G = \frac{2\pi}{\{(\frac{1}{a})-(\frac{b}{2})-(\frac{1}{a})+(\frac{b}{2})-(\frac{1}{a})+(\frac{b}{2})-(\frac{1}{a})+(\frac{b}{2})\}}$ (9)

that is, $G=\pi\left(\frac{a^2}{b}-\frac{b}{4}\right)$ (10)

Equation (10) gives the geometric factor of the Schlumberger array (Ishola *et al.*, 2016).

The apparent resistivity for the Schlumberger array is therefore gotten as

$$\rho_a = \pi R\left(\frac{a^2}{b}-\frac{b}{4}\right) \quad (11)$$

where a denote the half array length and b likewise denote the spacing between the potential electrodes (Figure 4). The apparent resistivity (ϱ_a) values of VES points were thereafter obtained by increasing the field resistance (R_a) values with suitable geometric factor in equation (11). The VES resistivity data were first processed by plotting the ϱ_a values against half- current electrode spacing (AB/2) on bi-logarithm graph paper and later presented as sounding curves (Aizebeokhai et al., 2016). Quantitative explanation of the achieved VES curves were done by partial curve matching, followed by computer-assisted 1D forward modelling technique (Oyeyemi *et al.*, 2020). IPI2WIN and WinResist softwares were used to process the data and obtain the layer parameters (resistivity, thickness and depth) from the field processes of VES data.

Groundwater Sample Collection

Samples of the water from hand-dug wells and borehole water were collected from different residential houses in duplicate in clean 2L PVC bottles to determine the physical and chemical parameters of water samples within the study area. At each sampling point, sampling bottle was rinsed thrice with the water to be collected prior to the real collection of the sample (Egbueri, 2020). Water samples for HMs analysis were collected inside 1-L PVC bottles (Egbueri and Mgbenu, 2020). After the collection of the water samples, the cap of each sample bottle was screwed on tightly in order to prevent seepage (Ganiyu et al., 2018). At the laboratory, a 0.45 µm filter was used to remove undesirable materials from the collected water samples (Ganiyu *et al.*, 2021). The collected water samples were later kept at 4^0C inside the fridge prior to the commencing of chemical analysis. In-situ determination for physical parameters such as taste and turbidity were measured using turbidity meter. Temperature, pH, Total Dissolved Solids (TDS) and Electrical Conductivity (EC) were measured on the field using multipurpose conductivity meter and colour comparator for pH. The concentration of major ions and elements including heavy metals such as iron (Fe^{+2}), copper (Cu^{+2}), zinc (Zn^{2+}), magnesium (Mg^{2+}), sodium (Na^{+}), potassium (K^{+}), calcium (Ca^{+2}), chloride (Cl^{-}), nitrate (NO_3^-), sulphate (SO_4^{2-}), carbonate (CO_3^-) and bi-carbonate (HCO_3^-) were determined using standard laboratory analyses. The concentrations of physical and chemical analyses results summary were presented in a table and compared with standard guideline limits of NSDWQ (2015) and WHO (2017) for safe drinking water. The water quality data was further subjected to Pearson correlation analysis to study the interrelationship between the analyzed parameters. Graphical representation in order to decipher hydrogeochemical facies of the sampled waters was done using Piper-trilinear diagram. Piper diagrams combine anion and cation in triangles which lie on a common baseline. The diamond shape between them was utilised to provide a preliminary judgement on the origin of the water represented by the study and to characterise various water types (Piper, 1944).

RESULTS AND DISCUSSION

Interpretation of 2D ERT Data

The 2D ERT data of the study area were inverted using the RES2DINV software as proposed by Loke and Barker (1996) to generate 2D resistivity inverse models beneath each of the six traverses. The results of the interpretation are as follows:

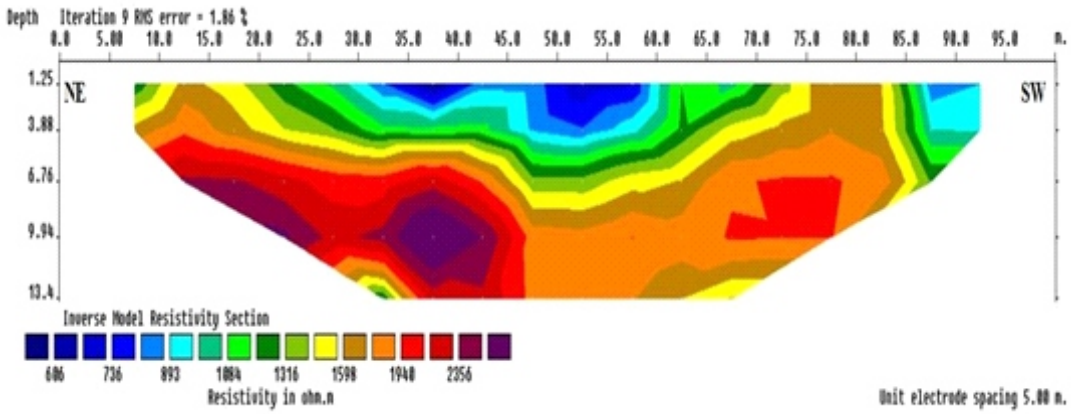

Figure 5. 2D Inverse Model Resistivity Section, Traverse 1.

Figure 5 shows the 2-D section of Traverse 1. The upper part reveals the inhomogeneity along the topsoil with resistivity values ranging between 606 and 1598 Ωm. An isolated conductive zone (< 1000 Ωm) with a thickness of about 4 m extends from the lateral distance 50 to 60 m along the traverse. A relatively dry exposed soil with resistivity value between 1598 to 1940 Ωm with a depth of more than 7 m was noticed from lateral distance 75 to 80 m along the traverse. A relatively shallow weathered layer with resistivity value between 1884 to 1598 constitute the second region. The third layer (highly resistive basement rock) with resistivity varying from 1900 to 2400 Ωm is observed from a depth of 5m downward at a lateral distance 10 to 45 m along the traverse.

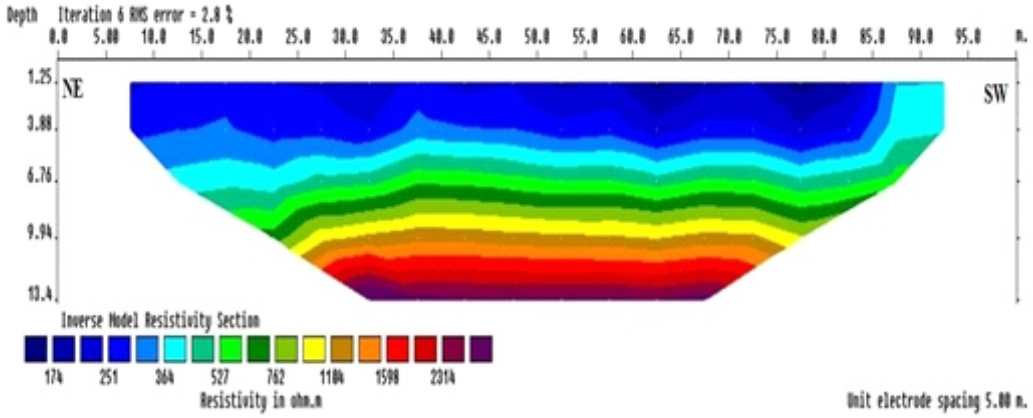

Figure 6. 2D Inverse Model Resistivity Section, Traverse 2.

Figure 6 shows the 2-D section of Traverse 2. The first layer (topsoil) on the traverse is about 7 m thick with resistivity varying from 174 to 364 Ωm. The second geologic layer is about 2 m thick and has a resistivity varying from 527 to 762 Ωm and classified as weathered basement (groundwater bearing zone). A resistive third layer (fresh basement) is observed at a depth of 10 m with resistivity varying from 1104 to 2400 Ωm.

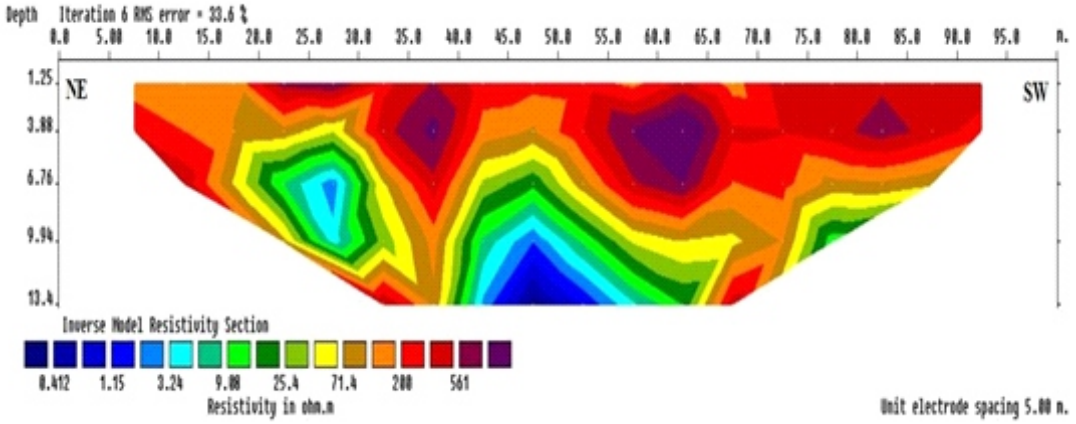

Figure 7. 2D Inverse Model Resistivity Section, Traverse 3.

Figure 7 shows the 2-D section of Traverse 3. The first layer on the traverse is relatively resistive topsoil with resistivity values ranging between 200 and 600 Ωm with a thickness of about 9 m. An isolated weathered conductive zone and an inverted V –shaped weathered basement region (with resistivity < 100 Ωm) and of variable thickness ranging from 6 - 10 m were observed at lateral distances 20 -35 m and 40 to 68 m, respectively along the traverse. These two regions constitute groundwater accumulation zones.

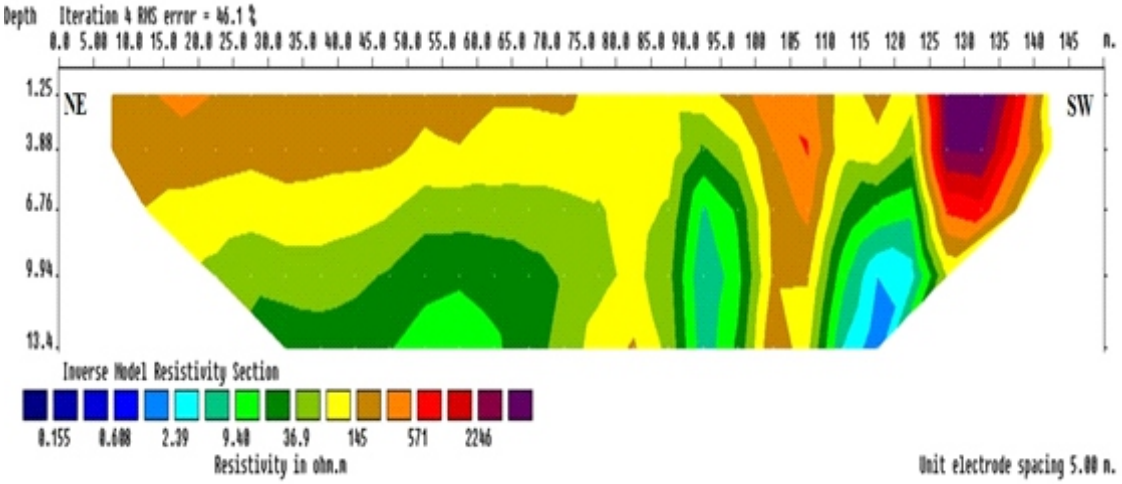

Figure 8. 2D Inverse Model Resistivity Section, Traverse 4.

Figure 8 shows the 2-D section of Traverse 4. The resistivity depth model section displays inhomogeneous topsoil layer of resistivity 145 - 2246 Ωm traverses the whole profile and descends to thickness that varied from 6 to 13 m, indicating thick overburden. Highly near surface resistive region (571 - 2246 Ωm with a thickness of about 10 m was observed towards the tail end of the traverse. Beneath this horizon is a weathered basement materials (<150 Ωm) of variable thickness that ranges from 6 -13 m, suggesting a good water bearing zone.

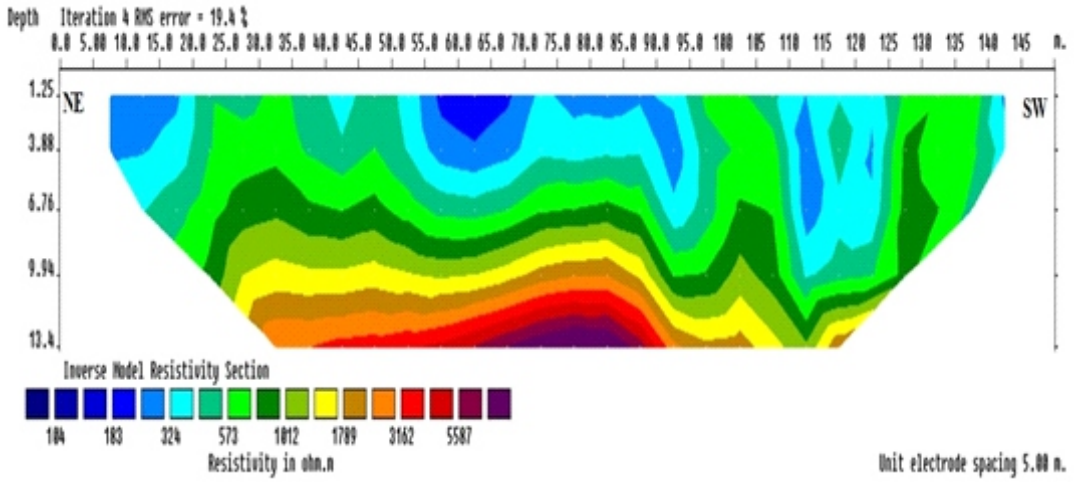

Figure 9. 2D Inverse Model Resistivity Section, Traverse 5.

Figure 9 shows the 2-D section of Traverse 5. From the 2-D section, there is steady rise in resistivity value with depth. The 2D section of traverse 5 shows three distinctive resistivity anomalies zones. The first zone (topsoil) has resistivity ranging from 104 - 573 Ωm with an average thickness of about 10 m, suggesting water bearing zone. This zone was observed to stretches far more extensively from the starting point 0 m to the end of the traverse. The second layer (weathered basement) was noticed at lateral distances 20 to 50 m, 95- 110m and from 126 m to the end of the traverse, with the resistivity varying from 573 -1012 Ωm and interpreted as a weathered layer with high recharge potential. This region is good potential for groundwater exploration because of its large size. Beneath this layer is a fresh basement with resistivity values of 1789 to 5587 Ωm, obtained at lateral distance 30 – 90 m of the traverse from a depth of 10.5 to 13.4 m.

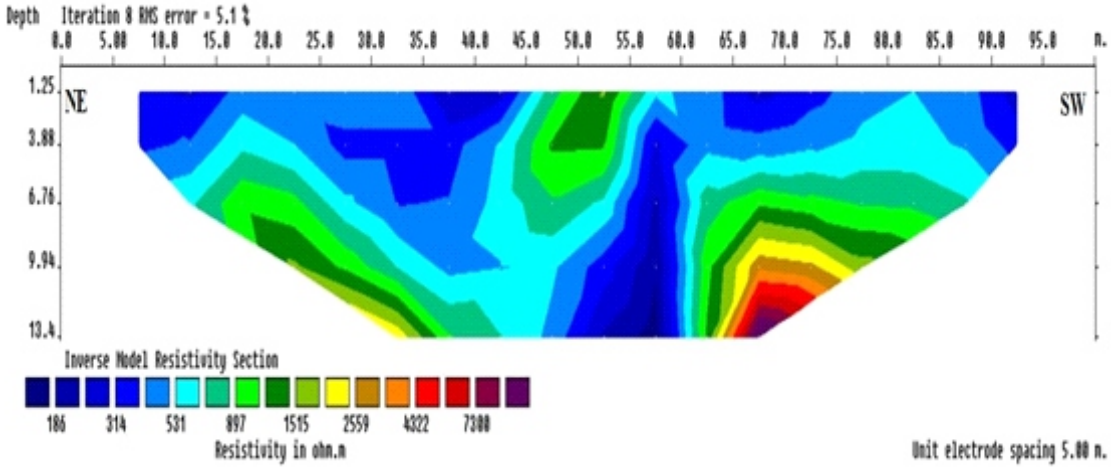

Figure 10. 2D Inverse Model Resistivity Section, Traverse 6.

Figure 10 shows the 2-D section of Traverse 6. The top layer on the traverse has resistivity varying from 180 to 530 Ωm and is of variable thickness. The second layer is a weathered basement, the first one was noticed at depth of 7m at lateral distance 10 -30 m of the traverse while second weathered region is of about 9 m thick with resistivity varying from 890 to 1515 Ωm. The third layer (basement) is observed towards the tail end of the traverse at 10 m depth with values of resistivity varying from 2559 to 7300 Ωm.

Interpretation of VES Data

The VES data were interpreted using IPI2WIN

and WinResist software. The results and salient features of the subsurface parameters are shown in Table 1. The curve types observed in the area consist of 3-layer H-type (8.3%) and K-type (16.7%); 4-layer HA-type (16.7%), HK-type (25%), QH-type (8.3%), QQ-type (8.3%) and AK-type (8.3%); and 5-layer HKH-type (8.3%). The HK-type is the most predominant curve in the area.

Table 1: Summary of VES Results.

VES Station/ Curve Type	No. of Layer	Resistivity (Ωm)	Thickness (m)	Depth (m)	Lithology
1	1	169.3	0.7	0.7	Topsoil
HA	2	45.0	0.7	1.4	Clayey soil
	3	566.7	17.6	19.0	Weathered basement
	4	3850.1	-	-	Fresh basement
2	1	2449.0	0.3	0.3	Topsoil
H	2	289.2	5.2	5.5	Clayey sand
	3	2352.3	-	-	Fresh basement
3	1	21194.7	0.1	0.1	Topsoil
HK	2	211.1	4.6	4.8	Clayey sand
	3	4030.6	11.9	15.6	Fresh basement
	4	15.0	-	-	Clayey soil
4	1	612.3	0.4	0.4	Topsoil
HK	2	464.9	4.5	4.9	Sandy soil
	3	5507.3	10.8	15.7	Fresh basement
	4	42.1	-	-	Clayey soil
5	1	314.2	0.7	0.7	Topsoil
HKH	2	97.4	0.9	1.5	Clayey soil
	3	270.1	1.7	3.3	Clayey sand
	4	19.8	27.3	30.6	Weathered basement
	5	3941.9	-	-	Fresh basement
6	1	557.4	2.3	2.3	Topsoil
QH	2	432.7	9.3	11.6	Sandy soil
	3	20.7	14.8	26.4	Weathered basement
	4	9088.8	-	-	Fresh basement
7	1	2815.7	0.5	0.5	Topsoil
QQ	2	606.1	3.6	4.1	Sandy soil
	3	167.0	24.1	28.1	Weathered basement
	4	145.3	-	-	Fractured basement
8	1	1338.0	1.2	1.2	Topsoil
HK	2	143.6	1.3	2.4	Clayey sand
	3	1963.1	4.2	6.6	Fresh basement
	4	2.4	-	-	Clayey soil
9	1	200.4	0.8	0.8	Topsoil
K	2	911.6	11.5	12.4	Weathered basement
	3	3.6	-	-	Clayey soil
10	1	100.1	0.5	0.5	Topsoil
AK	2	145.0	2.6	3.1	Clayey sand
	3	10898.0	1.1	4.2	Fresh basement
	4	1024.9	-	-	Fractured basement
11	1	240.1	0.3	0.3	Topsoil
HA	2	46.2	0.6	0.9	Clayey soil
	3	690.4	11.6	12.6	Weathered basement
	4	5648.8	-	-	Fresh basement
12	1	315.1	1.2	1.2	Topsoil
K	2	1880.7	22.7	23.9	Fresh basement
	3	579.4	-	-	Fractured basement

Geoelectric Section

The interpreted VES results were further used in constructing the geo-electrical sections. Typical geoelectric sections generated from the geoelectric parameters are shown in Figure 11, 12 and 13.

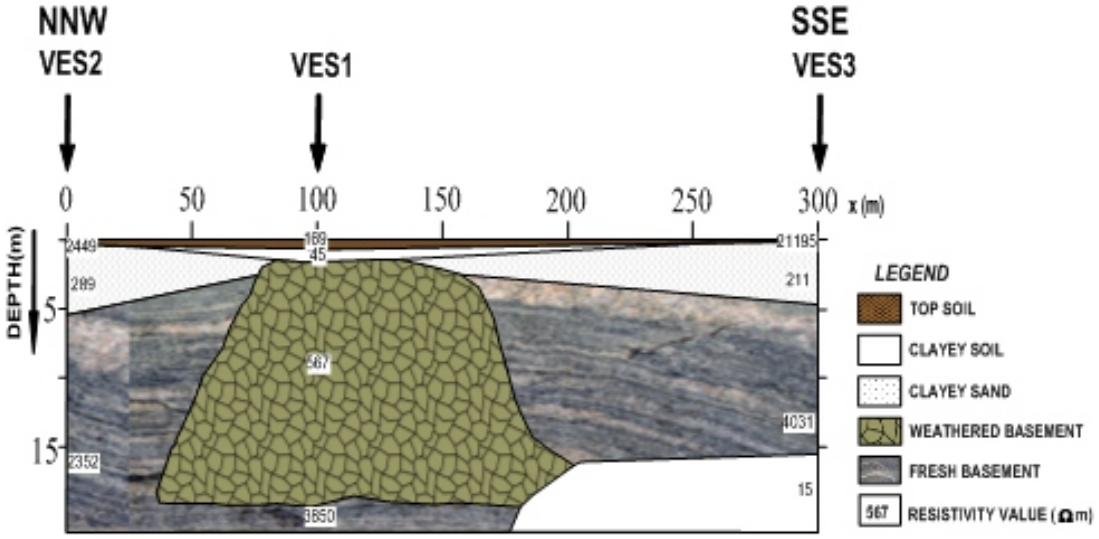

Figure 11: Geoelectric Section along Traverse 1 (VES 1, VES 2 and VES3).

Figure 11 gives the description of the subsurface sequence of rocks beneath Traverse 1 which contains VES 1, VES 2 and VES 3. Five lithological layers were identified beneath the traverse namely: topsoil, clayey soil, clayey sand, weathered basement and fresh basement from top to bottom. The topsoil resistivity and thickness vary from 169 to 211945 Ωm and 0.1 to 0.7 m respectively. The clayey soil resistivity and thickness is 45 Ωm and 0.7 m respectively. Clayey sand resistivity and thickness varies from 211 to 289 Ωm and 4.6 to 5.2 m respectively. The weathered basement resistivity and thickness are 567 Ωm and 17.6 m. The fresh basement resistivity vary from 2352 to 4031 m.

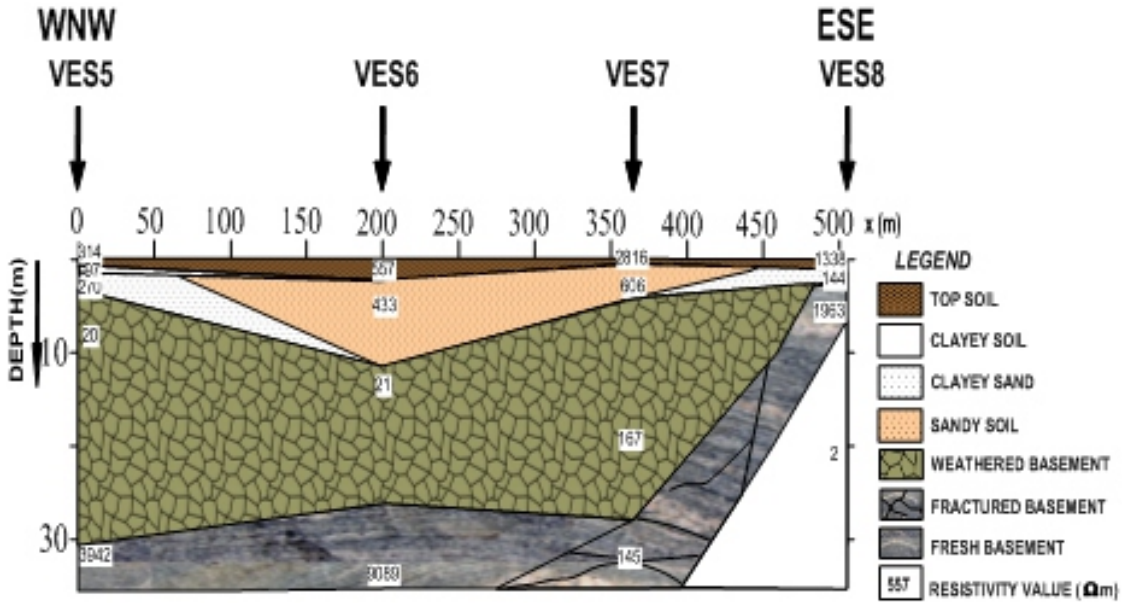

Figure 12: Geoelectric Section along Traverse 2 (VES 5, VES 6, VES 7 and VES 8).

Figure 12 gives the description of the subsurface sequence of rocks beneath Traverse 2 which contains VES 5, VES 6, VES 7 and VES 8. Seven lithological layers were identified beneath the traverse namely: topsoil, clayey soil, clayey sand, sandy soil, weathered basement, fractured basement and fresh basement from top to bottom. The topsoil has resistivity and thickness varying from 314 to 2816 Ωm and 0.5 to 2.3 m respectively. Clayey soil resistivity and thickness are 97 Ωm and 0.9 m. Sandy soil resistivity and thickness vary from 433 to 606 Ωm and 3.6 to 9.3 m respectively. Clayey sand resistivity and thickness vary from 144 to 270 Ωm and 1.3 to 1.7 m. The weathered basement resistivity varies from 20 to 167 Ωm. Fractured basement of resistivity is 145 Ωm while the fresh basement resistivity vary from 3942 to 9089 Ωm.

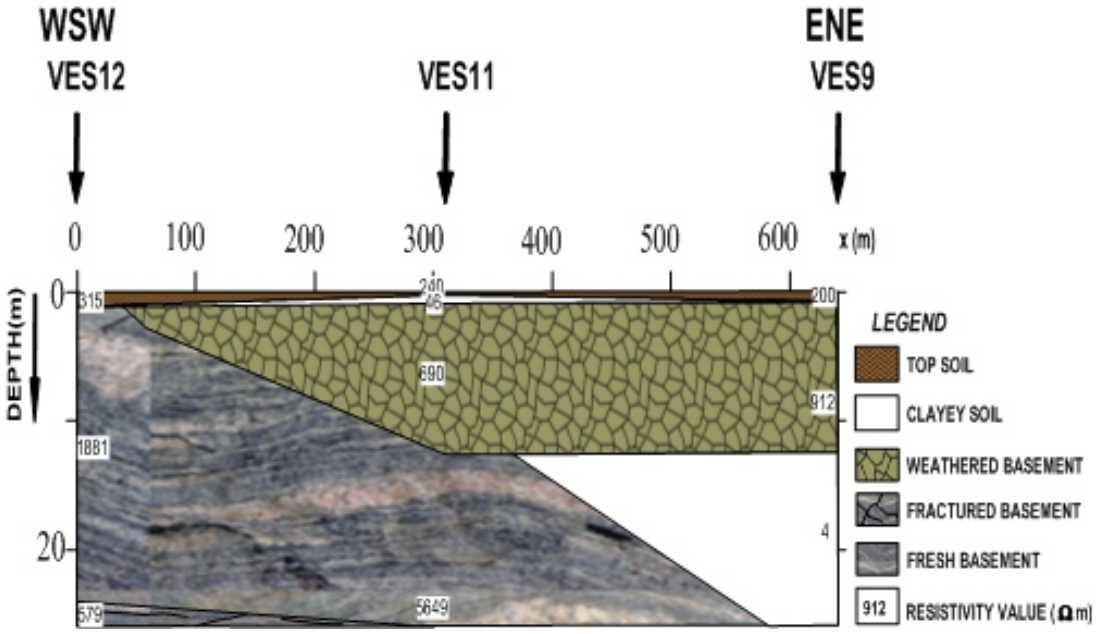

Figure 13: Geoelectric Section along Traverse 3 (VES 9, VES 11 and VES 12).

Figure 13 gives the description of the subsurface sequence of rocks beneath Traverse 3 which contains VES 9, VES 11 and VES 12. Five lithological layers were identified beneath the traverse namely: topsoil, clayey soil, weathered basement, fractured basement and fresh basement from top to bottom. The topsoil has resistivity and thickness varying from 200 to 315 Ωm and 0.3 to 1.2 m respectively. Clayey soil resistivity and thickness is 46 Ωm and 0.6 m respectively. The weathered basement has resistivity and thickness varying from 690 to 912 Ωm and 11.5 to 11.6 m. Fresh basement resistivity and thickness vary from 1881 to 5649 Ωm and 22.7 m. Fractured basement resistivity is 579 Ωm.

Evaluation of Aquifer Protective Capacity

The longitudinal unit conductance of the overburden rock units in a region is used to characterise aquifer protective capacity (Ugwu *et al.,* 2016). The first order geoelectric parameters (layer thicknesses and resistivities), which comprise Total Transverse Unit Resistance (T), Total Longitudinal Unit Conductance (S), and Coefficient of Anisotropy (λ), may be used to determine the Dar-Zarrouk parameters. These secondary geoelectric parameters are especially essential when utilised to define a multi-layered geoelectric section (Ogungbemi *et al.,* 2013). The combination of thickness and resistivity in the Dar-Zarrouk parameter can be used to study aquifer vulnerability.

The Total Longitudinal Unit Conductance for n layers is determined using

$$S = \sum_{i=1}^{n} \frac{hi}{\rho i} = \frac{h1}{\rho 1} + \frac{h2}{\rho 2} + \ldots\ldots + \frac{hn}{\rho n} \text{ (Siemens)} \quad (12)$$

The Total Transverse Unit Resistance is equally obtained using

$$T = \sum_{i=1}^{n} hi\rho i = h1\rho 1 + h2\rho 2 + \ldots. + hn\rho n \ (\Omega m^2) \quad (13)$$

=

Where hi represent the layer thickness, ϱi represent layer resistivity while the number of layers from the surface to the top of aquifer varies from $i = 1$ to n.

Coefficient of Anisotropy is calculated using

$$\lambda = (\varrho_T/\varrho_L)^{1/2} \quad (14)$$

where ϱ_T is the average transverse resistivity and ϱ_L is the average longitudinal resistivity.

For homogeneous isotropic media, $\lambda = 1$, whereas it ranges from 1 to 2 in homogeneous anisotropic media in which ϱ_T is greater than ϱ_L (Iduma *et al.*, 2016)

Table 2: Computed Aquifer and Dar-Zarouk Parameters of the Geoelectric Section.

VES Station	Aquifer Resistivity (Ωm)	Aquifer Thickness (m)	Aquifer Depth (m)	Longitudinal Conductance (S)	Transverse Resistance (Ωm^2)	Protective Capacity Rating
VES 1	4631.1	19.0	21.1	0.051	10123.93	Poor
VES 2	5090.5	5.5	5.8	0.018	2238.54	Poor
VES 3	25451.4	16.6	20.5	0.025	51054.67	Poor
VES 4	6626.6	15.7	21.0	0.013	61615.81	Poor
VES 5	4643.4	30.6	36.1	1.396	1307.31	Good
VES 6	10099.6	26.4	40.3	0.740	5612.49	Good
VES 7	3734.1	28.2	32.7	0.150	7614.51	Weak
VES 8	3447.1	6.7	10.2	0.012	10037.30	Poor
VES 9	1115.6	12.3	13.2	0.017	10643.72	Poor
VES 10	12168.0	4.2	7.8	0.023	12414.85	Poor
VES 11	6625.5	12.5	13.8	0.031	8108.39	Poor
VES 12	2775.2	23.9	25.1	0.016	43070.01	Poor

Table 2 shows the computed aquifer and Dar-Zarouk parameters of the geoelectric section. The values of longitudinal unit conductance (S) in the research area vary from 0.012 to 1.396 S. Clayey overburden gives protection to the underlying aquifer due to its relatively high longitudinal unit conductance. The areas having conductance values less than 0.1 S covers about 75% of the study area and was classified as zones of poor protective capacity, the values between 0.1 and 0.19 S covered about 8% and was classified as zone of weak protective capacity while about 17% of the area having conductance values between 0.7 and 4.9 S was considered to be of good protective capacity.

Groundwater Sample Analysis

Table 3: Result of Physical and Chemical Analyses of Some Selected Wells in Obada-Oko Area.

Chemical Parameters	S1	S2	S3	S4	S5	Mean	SD	NSDWQ 2007	WHO 2017
Ph	7.70	7.79	8.00	8.16	8.10	7.95	0.20	6.50 – 8.50	6.50 – 8.50
EC (µs/cm)	1000	100	2700	3600	2000	1880	2690	1000	1000
Temp. (^{0}C)	30.2	31.0	30.9	30.8	30.4	30.7	0.3	-	-
TDS (mg/L)	186.1	34.9	354.1	113.2	273.4	192.3	126.3	500.0	500.0
Turb (mg/L)	0.0	0.0	0.0	0.0	0.0	0.0	0.0	-	5.0
Ca^{2+} (mg/L)	10.358	0.471	17.417	2.849	11.813	8.581	6.898	-	75.000
Mg^{2+}(mg/L)	0.447	0.222	1.363	0.332	1.344	0.741	0.564	0.200	50.000
K^{+}(mg/L)	1.22	0.20	2.24	0.53	2.65	1.37	1.06	-	55.00
Na^{+} (mg/L)	5.05	1.81	6.56	4.25	3.48	4.23	1.77	200.00	50.00
Fe^{2+} (mg/L)	0.000	0.000	0.160	0.130	0.195	0.097	0.091	0.300	0.300
Cu^{2+} (mg/L)	0.0	0.0	0.0	0.0	0.0	0.0	0.0	1.0	1.0
Zn^{2+} (mg/L)	0.012	0.000	0.000	0.000	0.000	0.002	0.005	3.000	5.000

Table 3 shows the result of physical and chemical analyses of some selected wells in Obada-Oko area compared with NSDWQ (2007) and WHO (2017). The result indicated that the groundwater examined is slightly alkaline (pH: 7.95±0.20). It is mostly fresh with Total Dissolved Solid (TDS) of between 34.9 – 354.1 mg/L and an average TDS value of 192.3±126.3 mg/L which is less than 1000 mg/L, the value for fresh water (Oloruntola and Adeyemi, 2014). The values of groundwater temperature in the study area ranged from 30.2 – 31.0°C, having an average value of 27.7°C. This suggests that the groundwater temperature is generally ambient and good for consumers who prefer cool to warm water. High temperatures increase the proliferation of microorganisms, which has a detrimental effect on the quality of the water (Oyem *et al.,* 2014).

The electrical conductivity (EC) value in the groundwater varies from 100 – 3600 μs/cm having an average value of 1880±2690 μs/cm. This was due to the low water level in dry season, contributing to higher conductivity level in groundwater (VIMS, 2005).The groundwater is not cloudy as turbidity was undetectable. Ca^{2+}, Mg^{2+}, K+ and Na^{+} have average values of 8.581±6.898 mg/L, 0.741±0.564 mg/L, 1.37±1.06 mg/L and 4.23±1.77 mg/L respectively. They are all within maximum permissible level of WHO and NSDWQ except for Mg^{2+} (>0.200 mg/L). $Fe^{2+}$was undetectable in S1 and S2 with an average value of 0.097±0.091 mg/L. Cu^{2+} was undetectable in the entire water sample while Zn^{2+} was only present in S1 with 0.012 mg/L. CO_3^- and NO_3^- were also undetectable in the entire water sample. HCO_3^-, Cl^- and SO_4^{2-} have an average value of 87.90±23.46 mg/L, 63.38±15.61mg/L and 0.362±0.207 mg/L respectively. They are all within the maximum permitted level recommended by WHO and NSDWQ.

Correlation Coefficient Analysis

Table 4: Result of Correlation Coefficient of Obada-Oko Groundwater Sample.

	HCO_3	Cl	SO_4	Ca	Mg	K	Na	Fe	Zn	TDS	pH	EC	Temp
HCO_3	1												
Cl	-.108	1											
SO_4	.831**	-.246	1										
Ca	.184	-.597	.587	1									
Mg	.533	-.747*	.704*	.865**	1								
K	.321	-.786**	.505	.885**	.965**	1							
Na	.106	.000	.526	.802**	.502	.502	1						
Fe	.777**	-.327	.654*	.516	.794**	.725*	.354	1					
Zn	-.930**	.052	-.617	.144	-.292	-.077	.259	-.592	1				
TDS	.352	-.586	.670*	.979**	.931**	.927**	.772**	.681*	-.028	1			
pH	.800**	.073	.495	.117	.438	.343	.148	.891**	-.708*	.314	1		
EC	.582	.312	.488	.295	.362	.302	.560	.763*	-.360	.435	.854**	1	
Temp	.639*	.342	.498	-.381	-.181	-.431	-.236	.022	-.747*	-.307	.233	.079	1

**. Correlation is significant at the 0.01 level (2-tailed).

*. Correlation is significant at the 0.05 level (2-tailed).

Table 4 shows the result of the correlation analysis showing relationship among the parameters of water analyzed. The result reveals that HCO_3 has significant positive relation with SO_4 (r = 0.831), pH (r = 0.800) and Fe (r = 0.777) at 1% (p <0.01) level and has significant positive relation with temperature (r = 0.639) at 5% (p <0.05) level, while it has significant negative correlation with Zn (r = - 0.930) at 1% (p <0.01) level. These indicate that these salts are present in some groundwater samples. High positive correlation between Fe and HCO_3 shows that Fe is present in the groundwater as ferrous bicarbonate, $Fe(HCO_3)_2$. Dissolved carbon is distributed as a function of pH. Cl has significant negative correlation with K (r = - 0.786) and with Mg (r = - 0.747) at 1% (p <0.01) and 5% (p <0.05) levels respectively, this may be due to the presence of these metals as chloride in some groundwater samples.SO_4 has significant positive relation with

Mg (r = 0.704), Fe (r = 0.654) and TDS (r = 0.670) all at 5% (p <0.05) level. The correlation between Mg and Cl; Mg and SO_4 ions specify the rock-water interface dissolving and precipitation processes that have an impact on the chemistry of the groundwater (Al-Harbi*et al.,* 2009). Ca has significant positive correlation with Mg (r = 0.865), K (r = 0.885), Na (r = 0.802) and TDS (r = 0.979) all at 1% (p <0.01) level. Mg has significant positive correlation with K (r = 0.965), Fe (r = 0.794) and TDS (r = 0.931) at 1% (p <0.01) level. K has vital positive relation with TDS (r = 0.927) and Fe (r = 0.725) at 1% and 5% levels respectively. Na has significant positive correlation with TDS (r = 0.772) at 1% (p <0.01) level while Fe has significant positive relation with pH (r = 0.891) at 1% (p <0.01) level and with TDS (r = 0.681) and EC (r = 0.763) both at 5% (p <0.05) level. Fe is a transition element which has a specific stable range of pH in aqueous solution, hence the groundwater's redox state exerts clear influence on iron (Ngah and Nwankwoala, 2013). Zn has significant negative correlation with pH (r = -0.708) and temperature (- 0.747) both at 5% (p <0.05) level while pH has significant positive relation with EC (r = 0.854) at 1% (p <0.01) level.

Piper Trilinear Diagram

The Piper trilinear diagram is used to infer hydro-geochemical facies. The plots include two triangles, one for plotting cations and the other for plotting anions. The cation and anion fields are combined to show a single point in a diamond-shaped field, from which inference is drawn on the basis of hydro-geochemical facies concept (Sadashivaiah *et al.*, 2008). In the cation plot of the piper (Figure 14), 60% are of Calcium type while the remaining 40% are within ($Na^+ + K^+$) axis. None of the water samples fall within "no dominant" axis. In anion region of the plot, all the samples fall within the chloride axis, thus, they of chloride type. Further classification of the Piper trilinear diagram showed that alkaline earth ($Ca^{2+} + Mg^{2+}$) exceed alkalis ($Na^+ + K^+$) while strong acid ($SO_4^{2-} + Cl$) exceed weak acid (CO_3). From the plot, 20% are of CaMgCl type (S_1), 40% belong to NaCl type (S_2 and S_4) while the remaining 40% belong to $CaHCO_3$ type (freshwater; S_3 and S_5).

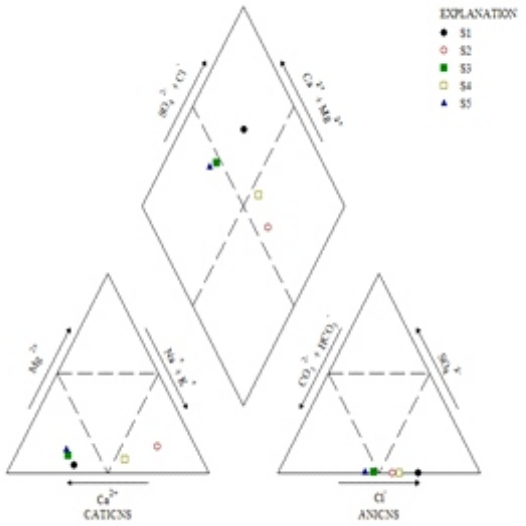

Figure 14: Piper Trilinear Diagram of Obada-Oko Groundwater Sample

CONCLUSION

The hydrogeophysical and groundwater quality of Obada-Oko community have been investigated. The profiles derived from 2D ERT have clearly delineated the various variations and distribution of resistivity laterally. The high and low resistivity zones are identified from the profiles. The resistivity varies from 0.155 Ωm along Traverse 4 and the highest bedrock resistivity of 7,300 Ωm along Traverse 6. Based on the subsurface resistivity distribution, the layers are dominated by high resistivity rock which indicates massive rock with highly resistive materials. Productive hand-dug wells/boreholes could be sited on Traverse 2, 3 and 6. The results of the vertical electrical sounding revealed the aquiferous zones and the

protective capacities of the overburden rock materials. VES 6 and VES 12 points have high groundwater potential. The longitudinal conductance revealed that the protective capacity rating of Obada-Oko falls in the poor to good category. VES 5 and VES 6 fall under good protective capacity rating indicating thick clayey layer which is protecting the underlying aquifer. VES 1, VES 2, VES 3, VES 4, VES 7, VES 8, VES 9, VES 10, VES 11 and VES 12 reveal low values of the protective capabilities of the overburden rock materials which make the aquifer system in the area highly vulnerable to contamination. The result from the physical and chemical analyses showed that the water samples are within maximum permissible level recommended by WHO and NSDWQ for drinking purposes. The result of Piper trilinear diagram shows the hydro-geochemical facies of the groundwater samples to be of CaMgCl, $CaHCO_3$ and NaCl water types in the study area. An important limitation to this research work is the absence of literature on this particular transition zone. A detailed study using other geophysical methods (which are faster and can cover wider area) should be employed to predict groundwater potential.

ACKNOWLEDGEMENT

The authors thank Prof. B. S. Badmus, Prof. A. O. Mustapha, Prof. (Mrs.) I. C. Okeyode and Dr. O. T. Olurin of Physics Department, Federal University of Agriculture, Abeokuta, Ogun State for their useful contributions and guidance towards the completion of this research study.

FUNDING

No fund was received for conducting this study.

CONFLICT OF INTEREST

The authors declare no competing interests.

AUTHOR CONTRIBUTION

Data acquisition and analysis were performed by V.M., S.A.G., B.S.B., O.A.I., J.O.O. and A.O.S. The authors contributed substantially to the conception.

REFERENCES

Adabanija**,** M. A. 2012.Hydrogeological Implications of Characteristics Features of Apparent Resistivity Curves, River Ogun Flood Plain, Ikorodu, Southwestern Nigeria**.** *International Journal of Scientific & Engineering Research*. 4 (10): 352-357.

Al-Harbi, O. A., Hussain, G. and Lafouza, O. 2009. Irrigation Water Quality Evaluation of Al-Mendasah Groundwater and Drainage Water, Al-Madenah Al-Monawarah Region, *Saudi Arabia*. *International Journal of Soil Science*. 4 (4): 123-141.

Aizebeokhai, A.P., Oyeyemi A.P., Oyeyemi, K.D., Joel, E.S. 2016. Groundwater potential assessment in a sedimentary terrain, Southwestern Nigeria. *Arab J Geosciences*, 9:496.
doi: 10.1007/s12517-016—2524-5.

Alile, M. O., Oranusi, S., Adetola, O. O. and Airen, J. O. 2012. Subsurface Geophysical Investigation and Physiochemical/Microbial Analysis of Groundwater Contaminant in Ota, Southwestern Nigeria. *Scientific and Academic Publishing* 2 (6): 176 - 184.

Alley, W., Reilly, T. E. and Franke, O. L. 1999. Sustainability of Ground-Water Resources. U.S. Geological Survey Circular 1186. Public domain.

Ariyo, S.O. and Banjo, A.A. 2008. Application of Electrical Resistivity Method for Groundwater Exploration in a Sedimentary Terrain: A Case Study of Ilara-remo, Southwestern Nigeria. *Continental Journal of Earth Sciences* 3: 53 – 58.

Badmus, B. S. and Olatinsu, O. B. 2012. Geophysical Characterization of Basement Rocks and Groundwater Potentials Using Electrical Sounding Data from Odeda Quarry Site, South-western, Nigeria. *Asian Journal of Earth Sciences* 5 (3): 79-87.

Boretti, A. and Rosa, L. 2019. Reassessing the Projections of the World Water Development Report. *npj Clean Water* **2,** 15 (2019).
doi: 10.1038/s41545-019-0039-9

Egbueri, J.C., Mgbenu, C.N. 2020. Chemometric analysis for pollution source identification and human health risk assessment of water resources in Ojoto Province, southeast Nigeria. *Applied Water Science,* 10:98.
doi: 10.1007/s13201-020-01180-9

Ganiyu, S.A., Badmus, B.S., Olurin, O.T. and Ojekunle, Z.O. 2018. Evaluation of seasonal variation of water quality using multivariate statistical analysis and irrigation parameter indices in Ajakanga area, Ibadan, Nigeria. *Appl. Water Sci*., 8:35.
doi: 10.1007/s13201-018-0677-y

Ganiyu, S.A, Mabunmi, A.A., Olurin. O.T., Adeyemi, A.A., Jegede, O.A., Okeh, A. 2021. Assessment of microbial and heavy metal contamination in shallow hand dug wells bordering Ona River, southwestern Nigeria. *Environ Monit Asses*, 193:126.
doi: 10.1007/s10661-021-08910-9

Greenburg, R 2005. The Ocean Moon: Search for an Alien Biosphere. Springer Praxis Books: 112

Hamill, L. and Bell, F.U. 1986. Groundwater Resources Development. *Britain Library Cataloguing in Publication Data, London*1: 151–158.

Iduma, R. E., Abam, T. K. and Etim Daniel Uko, E. D. 2016. Dar ZarroukParameter as a Tool for Evaluation of Well Locations in Afikpo and Ohaozara, Southeastern Nigeria. *Journal of Water Resource and Protection* 8: 505 – 521.

Ishola, S. A., Makinde, V., Aina, J. O., Ayedun, H., Akinboro, F. G., Okeyode, I. C., Coker, J. O. and Alatise, O. O. 2016. Aquifer Protection Studies and Groundwater Vulnerability Assessment in Abeokuta South Local Government Area, South-west Nigeria. *Journal of the Nigerian Association of Mathematical Physics*33: 347 - 362.

Jimoh, M., Bolarinwa,T. and Ashaye, O. 2015. Compositional Characteristics of the Migmatite Gneiss around Awo, Southwestern Nigeria. *Original Scientific Paper*.157-167.

Kearey, P., Brooks, M. and Hill, I. 2002. An Introduction to Geophysical Exploration.3rd Edition. *Blackwell Science* ISBN0632049294.

Kulshreshtha, S. N. 1998. A Global Outlook for Water Resources to the Year 2025. *Journal of Water Resources Management.* 12 (3): 167 – 184.
doi: 10.1023/A:1007957229865

Loke, M. and Barker, R. 1996. Rapid Least-squares Inversion of Apparent Resistivity Pseudosection by a Quasi-Newton Method. *Geophysical Prospecting* 44: 131-152.
doi:10.1111/j.1365-2478.1996.tb00142.x

Marshall, S. 2018. Electrical Methods - Resistivity Surveying. Appalachian State University. http://www.appstate.edu/~marshallst/GLY3160/lectures/12_Resistivity.pdf

Metwaly M. and Alfouzan F. 2013. Application of 2-D Geoelectrical Resistivity Tomography for Subsurface Cavity Detection in the Eastern Part of Saudi Arabia. *Geophysics Frontiers* 4 (4): 469 – 476.

Morris, B. L., Lawrence, A. R., Chilton, P. J., Adams, Calow, B. R. C. and Klinck, B. A. 2003. Groundwater and its Susceptibility to Degradation: A Global Assessment of the Problem and Options for Management. *Early Warning and Assessment Report Series, RS* 03: 3.

Ngah, S. A. and Nwankwoala, H. O. 2013. Iron (Fe^{2+}) Occurrence and Distribution in Groundwater Sources in Different Geomorphologic Zones of Eastern Niger Delta. *Archives of Applied Science Research*. 5 (2):266-272.

Nigerian Standard for Drinking Water Quality 2007. Nigerian Industrial Standard, Approved By: SON Governing Council. NIS 554: 2007.

Odunaya, A. A. 2012. Contribution of the "Cassava: Adding Value for Africa" Project to Income Generation in Nigeria: The Case of Cassava Farmers and Processors in Ewekoro Area of Ogun State. *Academic Journals*. 5 (9): 189 - 200.

Ogungbemi, O. S., Badmus, G. O., Ayeni, O. G. and Ologe, O. 2013. Geoelectric Investigation of Aquifer Vulnerability within Afe Babalola University, Ado – Ekiti, Southwestern Nigeria. *Journal of Applied Geology and Geophysics* 1 (5): 28 – 34.

Ogunsanwo, F. O., Olowofela, J. A. , Okeyode, I. C., O.A. Idowu, O. A. and O.T. Olurin, O. T. 2019. Aeroradiospectrometry in the Spatial Formation Characterization of Ogun State, South-western, Nigeria. *Scientific African Journal*. e00204.

Oli I. C., Okeke, O. C., Abiahu, C. M. G., Fagorite, V. I. and Anifowose, F. A., 2019. A Review of the Geology and Mineral Resources of Dahomey Basin, Southwestern Nigeria. International Journal of Environmental Sciences & Natural Resources. Juniper Publishers Inc. 21(1): 36-40

Oloruntola, M. O. and Adeyemi, G. O. 2014.Geophysical and Hydrochemical Evaluation of Groundwater Potential and Character of Abeokuta Area, Southwestern Nigeria. *Journal of Geography and Geology* 6 (3): 162 – 177.

Oyem, H., Oyem, M. and Ezeweali, D. 2014.Temperature, pH, Electrical Conductivity, Total Dissolved Solids and Chemical Oxygen Demand of Groundwater in Boji-BojiAgbor/Owa Area and Immediate Suburbs. *Research Journal of Environmental Sciences*8 (8): 444 – 450.

Oyeyemi, K.D., Aizebeokhai, A.P., Metwaly, M., Oladunjoye, M.A., Bayo-Solarin, B.A., Sanuade, O.A., Thompson, C.E., Ajayi, F.S., Ekhaguere, O.A. 2020. Evaluating the groundwater potwntial of coastal aquifer using geoelectrical resistivity survey and porosity estimation: A case in Ota, SW Nigeria. *Groundwater for Sustainable Development*.
doi: 10.1016/j.gsd.2020.100488

Piper, A. M. 1944. A Graphic Procedure in the Geochemical Interpretation of Water Analysis. *American Geophysical Union Transactions* 25: 914 – 923.

Radtke, D. B. 2002. Processing of Water Samples. U.S. Geological Survey TWRI 9 (2): 89.

Ravindran, A. A. and Prabhu, M. A. 2012. Groundwater Exploration Study Using Wenner-Schlumberger Electrode Array Through W-4 2D Resistivity Imaging Systems at Mahallipuram, Chennai, Tamilanadu, India. *Research Journal of Recent Sciences*1 (11): 36 – 40.

Sadashivaiah, C., Ramakrishnaiah, C. and Ranganna, G. 2008. Hydrochemical Analysis and Evaluation of Groundwater Quality in Tumbur Taluk, Karnataka State, India. *International Journal of Environmental Research and Public Health* 5 (3): 159.

Sassen, D. S., Hubbard, S. S., Bea, S. A., Chen, J., Spycher, N. and Miles E. Denham, M. E. 2012. Reactive Facies: An Approach for Parameterizing Field-scale Reactive Transport Models using Geophysical Methods. *Advancing Earth and Space Science*.
doi: 10.1029/2011WR011047

Schnug, E., Haneklaus, S. H., Hundhausen, U., Knolle, F., Jacobs, F. and Birke, M. 2019. Significance of Geographical, Hydrogeological, and Hydrogeochemical Origin for the Elemental Composition of Bottled German Mineral Waters. *Bottled and Packaged Water* 4: 277 – 310.

Sillanpää, M. and Shestakova, M. 2017. Classification of Pollutants and Water Treatment Methods. Electrochemical Water Treatment Methods. *47*.
doi: 10.1016/B978-0-12-811462-9.00002-5

Ufoegbune, G. C., Lamidi, K. I., Awomeso, J. A., Eruola, A. O., Idowu, O. A. and Adeofun, C. O. 2009. Hydro-geological Characteristics and Groundwater Quality Assessment in Some Selected Communities of Abeokuta, Southwest Nigeria. *Journal of Environmental Chemistry and Ecotoxicology* 1 (1): 10 – 22.

Ugwu, N., Simeon, R., Ranganai, R. and Ogubazghi, G. 2016. Geoelectric Evaluation of Groundwater Potential and Vulnerability of Overburden Aquifers at Onibu-Eja Active Open Dumpsite. *Journal of Water Resource and Protection*. doi: 10.4236/jwarp.2016.83026

UNICEF 2012. Progress on Drinking Water and Sanitation: 2012 Update. United States: WHO/UNICEF Joint Monitoring Programme for Water Supply and Sanitation.

United Nations 2009. The United Nations Water Development Project 3. *Water in Changing World*.

Virginia Institute of Marine Science. (2005). Physical Characteristics: Salinity in Shallow Water Habitats. Retrieved from http://web.vims.edu/bio/shallowwater/physical_characteristics/salinity.html

Ward, S. H. 1990. Resistivity and Induced Polarization Methods in Geotechnical and Environmental Geophysics. *Society of Exploration Geophysicists*1: 22.

World Health Organization 2011. Guidelines for Drinking Water Quality: Recommendations. Fourth Edition. Geneva: WHO.

World Health Organization 2017. Guidelines for Drinking Water Quality: Recommendations. Fourth Edition. Incorporating the First Addendum.

Zonge, K. 1993. Geophysical Prospecting Methods. *Zonge Engineering & Research Organization Tucson, AZ* 1: 34.